Transmission lines characteristic impedance versus Q-factor in CMOS technology

Johannes J.P. Venter[1] (ID), Anne-Laure Franc[2] (ID), Tinus Stander[1]
and Philippe Ferrari[3] (ID)

[1]Department for Electrical, Electronic, and Computer Engineering, Carl and Emily Fuchs Institute for Microelectronics, University of Pretoria, Pretoria, South Africa; [2]LAPLACE, University of Toulouse, CNRS, INPT, UPS, Toulouse, France and [3]RFIC-Lab, University of Grenoble Alpes, Grenoble, France

Abstract

This paper presents a systematic comparison of the relationship between transmission line characteristic impedance and Q-factor of CPW, slow-wave CPW, microstrip, and slow-wave microstrip in the same CMOS back-end-of-line process. It is found that the characteristic impedance for optimal Q-factor depends on the ground-to-ground spacing of the slow-wave transmission line. Although the media are shown to be similar from a mode of propagation point of view, the 60-GHz optimal Q-factor for slow-wave transmission lines is achieved when the characteristic impedance is ≈23 Ω for slow-wave CPWs and ≈43 Ω for slow-wave microstrip lines, with Q-factor increasing for wider ground plane gaps. Moreover, it is shown that slow-wave CPW is found to have a 12% higher optimal Q-factor than slow-wave microstrip for a similar chip area. The data presented here may be used in selecting Z_0 values for S-MS and S-CPW passives in CMOS that maximize transmission line Q-factors.

Introduction

Slow-wave transmission lines (SWTL) are promising building blocks for mm-wave integrated circuit (IC) designs in CMOS due to the high achievable transmission line Q-factors [1, 2]. For a required electrical length, a higher transmission line Q-factor results in lower loss, leading to more efficient circuits like couplers, filters and power dividers. The most common SWTLs investigated in literature are the slow-wave coplanar waveguide (S-CPW) [1–4] and a transmission medium designated by prior literature as slow-wave microstrip (S-MS) [5, 6]. The operating principles have been described in detail in prior literature [2, 4, 5], with some recent examples in literature [7–14] clearly illustrating its value in mm-wave CMOS circuit design.

S-CPW has been the topic of extensive parametric study for transmission line slow-wave factor and Q-factor [1, 15], as well as equivalent circuit modelling [3]. There has, however, not been a systematic comparison of S-CPW and S-MS in terms of (i) propagation mode, and (ii) Q-factor for comparable characteristic impedance (Z_0). Some studies have been carried out on the effect of Z_0 on Q-factor in slow-wave CPS (S-CPS) [15], but they did not elaborate on the methods or process geometry, and, to the best of the authors' knowledge, no measurement verification has been shown.

This paper presents the first comparative study on the propagating modes and effect of Z_0 on Q-factor for S-CPW and S-MS. The data presented here may be used to select Z_0 values for S-CPW and S-MS line components in CMOS circuits that maximise transmission line Q-factors. This may be valuable to the application of S-MS and S-CPW in designs where there is a need for low-loss transmission line sections, but freedom in the selection of Z_0. Examples include impedance matching networks [9], transmission zeros for filters [16], or tank resonators for mm-wave VCOs [14]. It also shows that these two types of SWTL are very similar in terms of propagation mode, despite the differentiating nomenclature established in literature. The analysis setup and transmission line geometries are discussed in Section II, followed by the simulation setup and measurement validation in Section III. The analysis of the mode propagation is carried out in Section IV. Results of the effect of Z_0 on the Q-factor are shown and discussed in Section V, and the paper concludes in Section VI.

Analysis setup

Parameter extraction

The symmetric transmission line ABCD parameters can be calculated from S-parameters, from which the parameters α, β, $\varepsilon_{r(eff)}$, γ, Q and Z_0 can be extracted using [12, 17]:

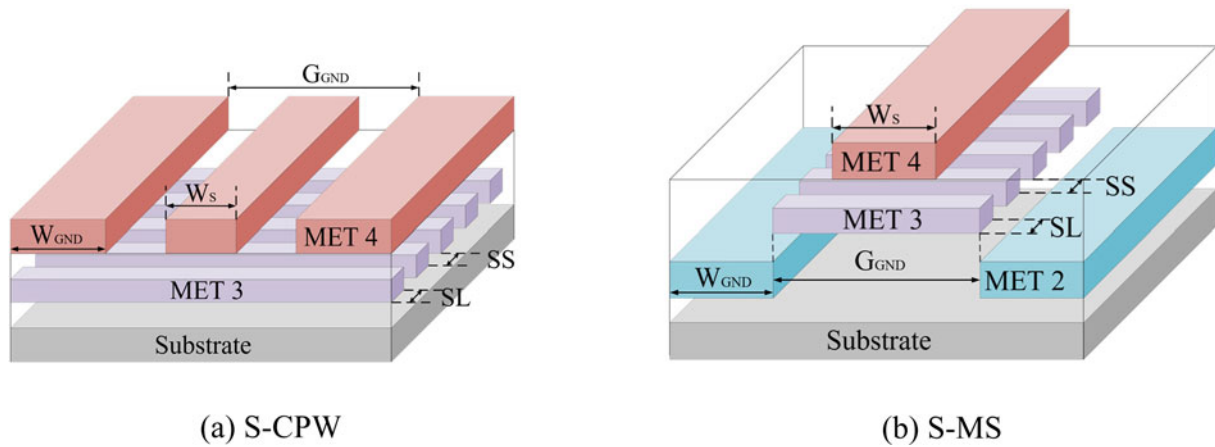$$\gamma = (\cosh^{-1}(A))/l \tag{1}$$

Fig. 1. Cross-sectional views of the slow-wave transmission line structures. (a) S-CPW (b) S-MS.

$$Z_0 = \sqrt{B/C} \qquad (2)$$

$$\alpha = 8.686 \cdot \Re(\gamma) \qquad (3)$$

$$\beta = (180/\pi) \cdot \Im(\gamma) \qquad (4)$$

$$Q = \beta/2\alpha \qquad (5)$$

$$\varepsilon_{r(eff)} = c_o^2 \cdot \left(\frac{1000 \cdot \beta}{\omega}\right)^2, \qquad (6)$$

where γ is the complex propagation constant, l the length (mm), Z_0 the characteristic impedance (Ω), α the attenuation constant (dB/mm), β the phase constant (degrees/mm), Q the quality factor, and $\varepsilon_{r(eff)}$ the effective relative permittivity.

Simulations were performed using the HFSS 3D FEM solver with the gap port inductance de-embedded [18]. The transmission lines were implemented in the AMS C35 process with four metal layers and thick M4 ($\approx$3 µm) option. All the simulated transmission lines have a length of 300 µm, which results from a compromise between the precision of the extracted attenuation constant (dB/m), and the inaccuracies in extracting characteristic impedance at frequencies where the line length approaches $\lambda/2$ electrical length (due to standing-wave effects).

Transmission line geometries

The slow-wave transmission lines under consideration are shown in Fig. 1. The CPW and S-CPW strips are implemented on the top metal layer (M4), with S-CPW using M3 for the shielding strip patterning (Fig. 1(a)). The microstrip uses M4 for the signal conductor and M2 for the ground plane, while the S-MS [5] uses M4 for the signal conductor, M3 for the shielding strip layer, and M2 for the slotted ground plane (Fig. 1(b)). This ensures similar separation between the shielding strips and the signal conductor in both S-CPW and S-MS lines, leading to comparable Z_0 ranges. The gap in the S-MS ground plane increases the linear inductance as compared to classical microstrip line, without changing the
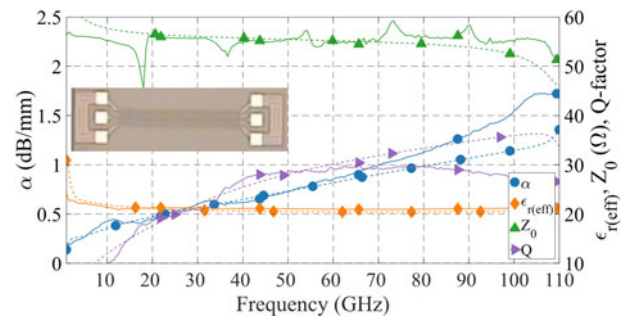
Fig. 2. Broadband validation of parameter extraction method for S-CPW1.

linear capacitance (resulting in a slow-wave behaviour), at the cost of increased chip area. By the same way, for the S-CPW, the shielding strip patterning leads to an increase of the linear capacitance, as compared to classical CPW without changing the linear inductance (resulting in a slow-wave behaviour), here again at the cost of increased chip area. This increase in inductance for S-MS lines and capacitance for S-CPWs may suggest that the propagation modes are different, but this is simply due to the reference taken for the linear inductance or capacitance increase, either microstrip or CPW. As already specified above, we show in section III that the two modes are in fact similar.

Measurement validation of simulation setup and extraction method

To validate the simulation approach, the S-CPWs from [1, 19] were simulated and compared to measurement results, extracting the transmission line parameters as described in Section II. Prototypes were characterized on an Anritsu VNA with GSG wafer probing, with the effects of probe pads de-embedded using the technique in [20]. The resulting comparison for S-CPW1 is shown up to 110 GHz in Fig. 2. The results at 60 GHz, for all four S-CPW geometries, are summarized in Table 1, and compare extremely well with the parameters extracted in [1, 19]. A maximum error of below 5% for $\varepsilon_{r(eff)}$ and below 16% for α is obtained in all cases, which are comparable to the measurement error. An increased error in α is evident above 70 GHz (also observed in [1]) and may be attributed to incomplete de-embedding of the

Table 1. Comparison of simulated and measured S-CPW parameters at 60 GHz to validate simulation approach.

S-CPW geometry (μm)	Parameter	Measured	Simulated	Error (%)
S-CPW1:	α (dB/mm)	0.86	0.82	4.7
$W_S = 7$; $G_{GND} = 107$; SL = 0.6; SS = 1; $W_{GND} = 10$	$\varepsilon_{r(eff)}$	21	20.5	2.4
S-CPW2:	α (dB/mm)	1.06	1.19	12.3
$W_S = 10$; $G_{GND} = 210$; SL = SS = 0.6; $W_{GND} = 60$	$\varepsilon_{r(eff)}$	37.3	36.4	2.4
S-CPW3:	α (dB/mm)	1.15	1.33	15.7
$W_S = 18$; $G_{GND} = 218$; SL = SS = 0.6; $W_{GND} = 60$	$\varepsilon_{r(eff)}$	50.5	48.0	5.0
S-CPW4:	α (dB/mm)	1.42	1.51	6.3
$W_S = 18$; $G_{GND} = 318$; SL = SS = 0.6; $W_{GND} = 60$	$\varepsilon_{r(eff)}$	56.5	57.6	2.0
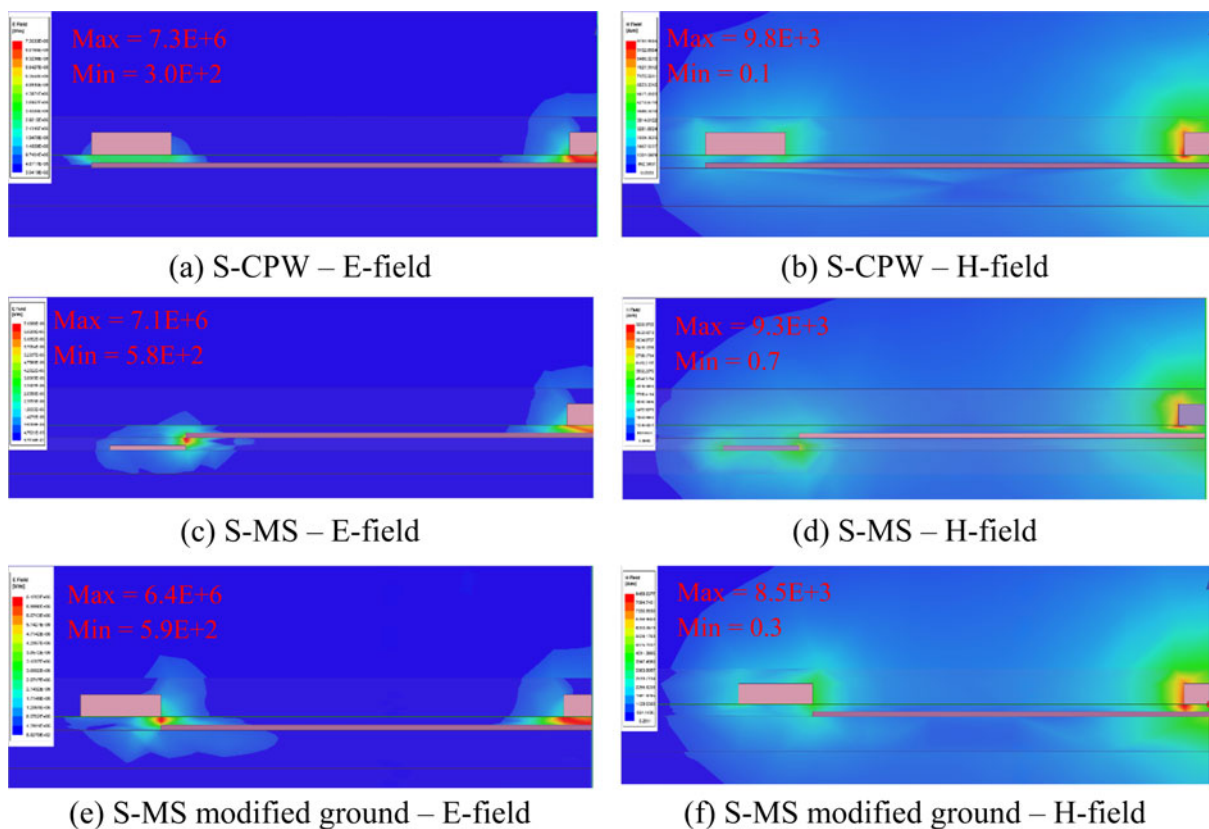
Fig. 3. SWTL field lines (a) S-CPW – E-field, (b) S-CPW – H-field, (c) S-MS – E-field, (d) S-MS – H-field, (e) S-MS modified ground – E-field, (f) S-MS modified ground – H-field.

tapered feed lines used in the S-CPW prototype [1]. Nevertheless, these results indicate good agreement between simulation and measurement for further analysis. All further results are presented at 60 GHz. Although the specific values presented here may differ at other frequencies and with different BEOL process stacks, it is found that the observed trends are also present in literature where similar parametric variations are applied [15, 21], though a systematic analysis to establish an optimal impedance for maximum Q-factor was not pursued in any of the prior studies.

Propagation mode analysis

In this section, we compare the propagation modes of S-CPWs and S-MS lines, based on the layouts shown in Fig. 1. The electric

and magnetic fields for each of these two lines are given in Figs 3(a)–3(d). Although the two media present similar magnetic field patterns, dissimilar electric field patterns are evident in Figs 3(a) and 3(c). However, if the location of the S-MS ground planes is modified, placing it coplanar with the signal strip, as shown in Figs 3(e) and 3(f), we obtain an electric field with a form similar to that of S-CPW. This leads to the conclusion that the S-CPWs studied in [1, 2] and the S-MS lines studied in [5, 7] propagate a very similar mode, despite the separate designations in prior literature. The distinguishing feature between the geometries is the width of the floating shield. For the transmission lines designated here (in keeping with prior literature [5]) as S-MS, the width of the floating shield is narrower, modifying the linear capacitance and enabling variation of characteristic

Table 2. Signal conductor width ranges for different G_{GND} values.

W_{GND} (μm)	G_{GND} (μm)	W_S (μm)
25	10	0.5–9.5
	30	0.5–25
	50	0.5–45
	80, 100, 120	0.5–60

impedance by modifying its width. This is demonstrated in Section V.

Results

With the validity of the simulation and extraction methods established by measurement, a large parametric simulation study was conducted. $W_{GND} = 25$ μm and $SS = SL = 0.7$ μm are kept constant, while G_{GND} is varied from 10 to 120 μm. To vary the characteristic impedance (Z_0), the signal strip width (W_S) is varied (Table 2). This allows for a wide Z_0 tuning range, from which design rules may be derived. As some geometries may violate

PDK layout rules multi-strips and dummy layout strategies may be required in some cases in order to implement these transmission lines.

Figure 4 shows the 60-GHz Q-factor versus Z_0 for S-CPWs versus ground-to-ground spacing G_{GND} and, consequently, required chip area. For comparison, standard CPWs of the same G_{GND} are also simulated. The peak Q-factor for standard CPW increases up to $G_{GND} = 30$ μm (reaching 14 for $Z_0 = 69$ Ω) and then decreases for larger G_{GND}. This is due to the electric field that increasingly penetrates the lossy bulk silicon substrate as G_{GND} increases. The narrow-gap S-CPW of $G_{GND} = 10$ μm exhibits a Q-factor comparable to the best-performing standard CPW, though the S-CPW Q-factor increases as G_{GND} increases, peaking above 30, similar to the trend observed in [21].

In the same way, the Q-factor versus Z_0 for the S-MS lines of various Z_0 values is shown in Fig. 5. For comparison, a standard microstrip line is also considered, achieving a peak Q-factor of 15.6 for Z_0 between 45 and 55 Ω. The S-MS line has a lower Q-factor compared to standard microstrip for small G_{GND} values but increases with increased G_{GND} as is the case with the CPW versus S-CPW comparison.

From the results in Figs 4 and 5, it is evident that the Z_0 for which peak Q-factor is achieved, lowers as G_{GND} increases (see
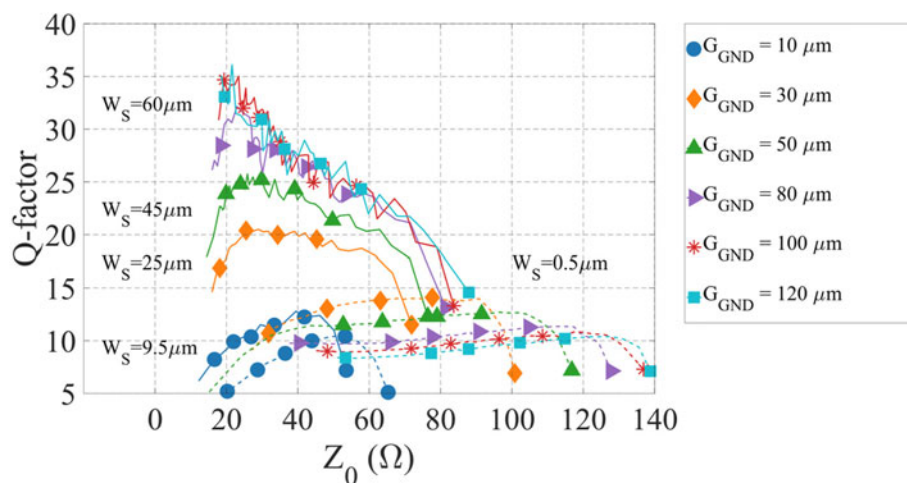

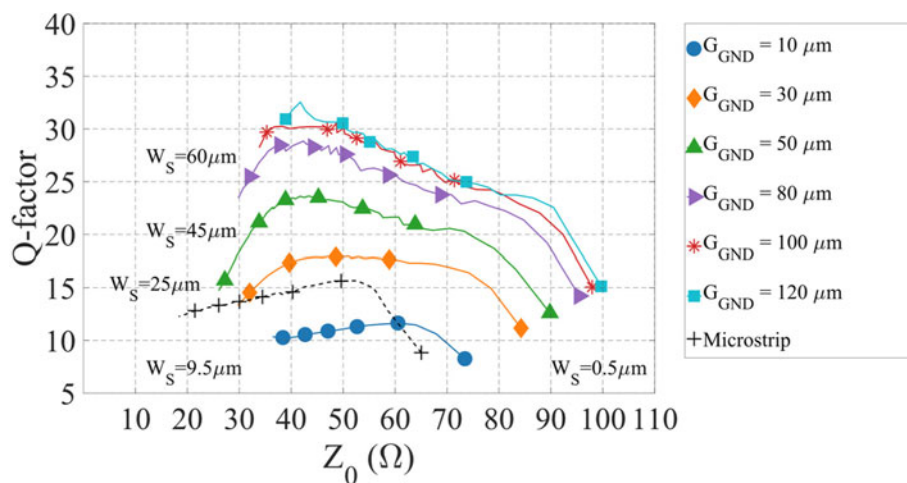**Fig. 4.** 60-GHz Q-factor versus Z_0 for CPW (dashed traces) and S-CPW (solid traces) for different G_{GND} values.

Fig. 5. 60-GHz Q-factor versus Z_0 of S-MS line for different G_{GND} values.

Fig. 6. Maximum Q-factor at 60 GHz (left) and Z_0 at max Q-factor (right) of S-CPW and S-MS for various G_{GND} values, with W_S indicated for each Z_0 value.

Fig. 7. Comparison of 60-GHz Q-factor for S-CPWs (blue) and S-MS lines (orange) for $G_{GND} \leq 50\,\mu m$.

Fig. 6), both for S-CPWs and S-MS lines (similar to the trend observed in [15]). The increase of the Q-factor when G_{GND} increases is due to the increase in the width of the strip W_s (see Fig. 6), which leads to a reduction in conductive losses, modeled by R_{strip}. However, when W_s becomes too large, for very low Z_0, the Q-factor decreases. This is mainly due to increase in the linear capacitance, as demonstrated in [2], since the attenuation constant α is proportional to the frequency squared times the linear capacitance (second term of the right term of the equation):

$$\alpha \approx \frac{1}{2} \cdot \frac{R_{strip} + R_{eddy}}{\sqrt{L_l/C_l}} + \frac{1}{2} \cdot \omega^2 \cdot R_p \cdot C_l \sqrt{L_l \cdot C_l} \qquad (7)$$

with R_{strip} the resistance of the strips (in Ω/m), R_{eddy} the equivalent resistance due to the eddy current losses in the shielding strips (in Ω/m), R_p the resistance of the shielding strips (in $\Omega \cdot$ m), and L_l and C_l the linear inductance (in H/m) and linear capacitance (in F/m) of the transmission line, respectively.

For S-CPW, the Z_0 for peak Q-factor varies from 40 to 23 Ω, while the S-MS optimum Z_0 varies between 61 and 40 Ω. There is, therefore, no global optimal Z_0 for peak Q-factor in either medium, but rather an optimum for a given value of G_{GND}.

Note that, when G_{GND} is larger than 50 μm, the uncertainty of the extracted Q-factor increases for the SWTLs, manifesting as a ripple in the traces in Figs 4 and 5. This may be attributed to remeshing noise in the high aspect ratio shielding strips [22]. Despite this variation, the trend is clearly evident.

Figure 6 compares the peak Q-factor and the associated Z_0 for various G_{GND} values. S-CPW achieves, on average, 12% higher Q-factor compared to S-MS. This is due to the higher sheet resistance of the reduced thickness M2 ground plane used for S-MS lines. The Z_0 associated with peak Q-factor equals 23 Ω and 43 Ω for S-CPWs and S-MS lines, respectively, indicating that so-called S-MS lines are preferred for $Z_0 >40\,\Omega$, and S-CPW for $Z_0 <40\,\Omega$.

For practical implementations, $G_{GND} >50\,\mu$m may be unacceptable, both because of the large occupied surface area as well as the resulting complexity of implementing T-junctions. Figure 7 shows the comparison of S-CPWs and S-MS lines for $G_{GND} \leq 50\,\mu$m, where it is again evident that S-CPW reaches a peak Q-factor for lower Z_0 compared to S-MS, and that S-CPW has a higher overall peak Q-factor compared to S-MS. From Fig. 7, it can further be concluded that S-MS is preferred for Z_0 higher than $\approx$50–60 Ω if narrow transmission line width is required. This conclusion provides a valuable design guideline

for CMOS designers wishing to integrate high Q-factor S-CPWs or S-MS lines in their circuits.

Conclusion

The propagation mode of S-CPW and S-MS have been analysed. It is found that the propagating modes are very similar, with S-MS exhibiting field patterns more similar to CPW than the microstrip field patterns described in [5, 7].

Next, the Q-factor of different on-chip transmission lines, as simulated in the AMS C35 process, have been evaluated as a function of their characteristic impedance. In general, the S-CPW is found to have a 12% higher Q-factor than S-MS lines in the same process. However, the Z_0 for which maximum Q-factor is achieved, reduces as the ground-to-ground spacing of the transmission lines increases, and differs between S-CPWs and S-MS lines. S-MS lines may, therefore, be preferred for certain values of Z_0, depending on the acceptable transmission line occupied surface area.

This analysis highlights the clear dependence between the transmission line characteristic impedance and Q-factor, and that the optimal Q-factor varies as the ground-to-ground spacing (and, subsequently, the on-chip area) changes. Future work will explore similar experiments for other kinds of CMOS slow-wave transmission lines, as well as derive suitable analytical or numerical models that capture the relationship between Z_0 and Q-factor.

References

1. **Cheung TSD and Long JR** (2006) Shielded passive devices for silicon-based monolithic microwave and millimeter-wave integrated circuits. *IEEE Journal of Solid-State Circuits* **5**, 1183–1200.
2. **Franc A-L, Pistono E, Meunier G, Gloria D and Ferrari P** (2013) A lossy circuit model based on physical interpretation for integrated shielded slow-wave CMOS coplanar waveguide structures. *IEEE Transactions on Microwave Theory and Techniques* **2**, 754–763.
3. **Bautista A, Franc A-L and Ferrari P** (2015) Accurate parametric electrical model for slow-wave CPW and application to circuits design. *IEEE Transactions on Microwave Theory and Techniques* **12**, 4225–4235.
4. **Kaddour D, Issa H, Franc A-L, Corrao N, Pistono E, Podevin F, Fournier J, Duchamp J and Ferrari P** (2009) High-Q slow-wave coplanar

transmission lines on 0.35 um CMOS process. *IEEE Microwave and Wireless Components Letters* **19**, 542–544.

5. **Amin NM, Wang Z and Li Z** (2015) A High Performance Slow-Wave Elevated Microstrip Line with Slot-Type Floating Shields, *2015 Asia-Pacific Microwave Conf. (APMC)*, Nanjing.

6. **Lee JJ and Park CS** (2010) A slow-wave microstrip line With a high-Q and a high dielectric constant for millimeter-wave CMOS application. *IEEE Microwave and Wireless Components Letters* **20**, 381–383.

7. **Kim K and Nguyen C** (2015) An ultra-wideband Low-loss millimeter-wave slow-wave Wilkinson power divider on 0.18 μm SiGe BiCMOS process. *IEEE Microwave and Wireless Components Letters* **25**, 331–333.

8. **Margalef-Rovira M, Lugo-Alvarez J, Bautista A, Vincent L, Lepilliet S, Saadi AA, Podevin F, Barragan MJ, Pistono E, Bourdel S, Gaquiere C and Ferrari P** (2020) Design of mm-wave slow-wave-coupled coplanar waveguides. *IEEE Transactions on Microwave Theory and Techniques* **68**, 5014–5028.

9. **Parveg D, Varonen M, Karaca D, Vahdati A, Kantanen M and Halonen K** (2018) Design of a D-band CMOS amplifier utilizing coupled slow-wave coplanar waveguides. *IEEE Transactions on Microwave Theory and Techniques* **66**, 1359–1373.

10. **Parveg D, Varonen M, Karaca D and Halonen K** (2019) Wideband mm-wave CMOS slow wave coupler. *IEEE Microwave and Wireless Components Letters* **29**, 210–212.

11. **Hwang J, Chu SH, Jeong GS, Youn Y, Kim W, Kim T and Jeong DK** (2020) A programmable On-chip reference oscillator With slow-wave coplanar waveguide in 14-nm FinFET CMOS, IEEE trans. *Circuits and Systems II: Express Briefs* **67**, 1834–1838.

12. **Lourandakis E, Nikellis K, Tsiampas M, Yamaura S and Watanabe Y** (2018) Parametric analysis and design guidelines for mm-wave transmission lines in nm CMOS. *IEEE Transactions on Microwave Theory and Techniques* **10**, 4383–4389.

13. **Galatro L, Pawlak A, Schroter M and Spirito M** (2017) Capacitively loaded inverted CPWs for distributed TRL-based De-embedding at (Sub) mm-waves. *IEEE Transactions on Microwave Theory and Techniques* **65**, 4914–4924.

14. **Sharma E, Saadi AA, Margalef-Rovira M, Pistono E, Barragan MJ, Lisboa de Souza AA, Ferrari P and Bourdel S** (2020) Design of a 77 GHz *LC*-VCO with a slow-wave coplanar stripline-based inductor. *IEEE Transactions on Circuits and Systems I: Regular Papers* **64**, 378–388.

15. **Horestani AK, Al-Sarawi S and Abbott D** (2010) Designing of High-Q Slow-Wave Coplanar Strips for CMOS MMICs, *35th Int. Conf. on Infrared, Millimeter, and Terahertz Waves*, Rome.

16. **Franc A-L, Pistono E, Gloria D and Ferrari P** (2012) High-Performance shielded coplanar waveguides for the design of CMOS 60-GHz bandpass filters. *IEEE Transactions on Electron Devices* **59**, 1219–1226.

17. **Vecchi F, Repossi M, Eyssa W, Arcioni P and Svelto F** (2009) Design of Low-loss transmission lines in scaled CMOS by accurate electromagnetic simulations. *IEEE Journal of Solid-State Circuits* **9**, 2605–2615.

18. ANSYS: ANSYS HFSS, 2020. [Online]. Available: https://www.ansys.com/products/electronics/ansys-hfss. [Accessed 2020].

19. **Franc A-L, Pistono E and Ferrari P** (2015) Dispersive Model for the Phase Velocity of Slow-Wave CMOS coplanar Waveguides, *2015 European Microwave Conf. (EuMC)*, Paris.

20. **Mangan A, Voinigescu S, Yang M and Tazlauanu M** (2006) De-embedding transmission line measurements for accurate modeling of IC designs. *IEEE Transactions on Electron Devices* **53**, 235–241.

21. **Tang X-L, Franc A-L, Pistono E, Siligaris A, Vincent P, Ferrari P and Fournier J-M** (2012) Performance improvement versus CPW and loss distribution analysis of slow-wave CPW in 65 nm HR-SOI CMOS technology. *IEEE Transactions on Electron Devices* **5**, 1279–1285.

22. **Lamecki A, Balewski L, Mrozowski M** (2016) Effect of Mesh Deformation on the Accuracy of 3D FEM Electromagnetic Analysis, *2016 IEEE MTT-S Int. Conf. on Numerical Electromagnetic and Multiphysics Modeling and Optimization (NEMO)*, Beijing.

Johannes J.P. Venter received the B.Eng. degree in Electronic Engineering, and the B.Eng.Hons. degree in Microelectronic Engineering from the University of Pretoria, Pretoria, South Africa, in 2015 and 2016, respectively. He is currently pursuing a Ph.D. degree in Electronic Engineering with the same institution. Since January 2021, he serves as RF/MMIC Engineer at Multifractal Semiconductors (Pty) Ltd.

Anne-Laure Franc received the engineer and M.Sc. degrees from the Cergy-Pontoise University, Paris, France, in 2008 and the Ph.D. degree from the Grenoble University, France, in 2011. In 2012, she had a postdoctoral position with the Darmstadt University, Germany and she held a temporary lecturer and research assistant position in the Grenoble-Alpes University, Grenoble, France in 2013. Since September 2013, she has been an assistant professor with the University of Toulouse, France. Her research interests focus on the design, modelling and miniaturization of tunable microwave components.

Tinus Stander received the B.Eng. and Ph.D. degrees in electronic engineering from the University of Stellenbosch, Stellenbosch, South Africa, in 2005 and 2009, respectively. From 2010 to 2012, he served as RF and Microwave Engineer at Denel Dynamics (a division of Denel SOC, Ltd.). He joined the Department of Electrical, Electronic, and Computer Engineering, Carl and Emily Fuchs Institute for Microelectronics, University of Pretoria, in 2013. He currently serves as a Principal Investigator in microwave and millimeter-wave microelectronics at the Institute, with personal research interest in the application of distributed passives on-chip and built-in self-testing. He is also registered as Professional Engineer with the Engineering Council of South Africa and serves as a Scientific Advisor with Multifractal Semiconductors (Pty) Ltd.

Philippe Ferrari received the Ph.D. degree from the "Institut National Polytechnique de Grenoble" (INPG), France, in 1992, with honors. Since 2004, he is a professor at the University Grenoble Alpes, Grenoble, France. His main research interest concerns tunable and miniaturized devices, such as filters, phase shifters, matching networks, couplers, power dividers and VCOs. These devices are developed in many technologies, PCB, CMOS/BiCMOS, and nanowires, at RF and mm-wave frequencies. He has worked towards the development of slow-wave CPW, and developed new topologies of slow-wave transmission lines, based on microstrip lines and SIWs, respectively. He is author or co-author of more than 230 papers published in international journals or conferences, and co-holder of six patents. He is an IEEE senior member, a member of the Editorial Board of the International Journal on RF and Microwave Computer-Aided Engineering (Wiley), an Associate Editor of the International Journal of Microwave and Wireless Technologies (EuMA) and member of the Editorial Board of *Electronics Letters*.